# Validation of Controller Approached Hysteresis Modelling with NiMH based Energy Storage Systems for use in xEVs

Sergej Koch[*], Thorsten Grün, Martin Doppelbauer

[*]*Sergej Koch (corresponding author) Karlsruhe Institute of Technology (KIT), Institute of Electrical Engineering (ETI), Hermann-von-Helmholtz-Platz 1, 76344 Eggenstein-Leopoldshafen, Germany; sergej.koch2@kit.edu*

## Summary

The State of Charge of current battery technologies cannot be measured directly and has to be estimated by using models along with measurable values like voltage, current and impedance.

Especially hysteresis effects caused by chemical and physical processes are increasing the complexity of the models to ensure still a high accuracy of State of Charge estimation (~2 % error)

In addition to state-of-the-art models, e.g. various models derived from the literature, a new widely customizable controller-based approach is presented in this work to reduce the general complexity of the highly discussed hysteresis and to make it more accessible to a broader field of experts.

*Keywords: Hysteresis, modelling, Controller, NiMH, SOC*

## 1 Introduction

The transition from conventional drive to electric mobility to reduce $CO_2$ emissions is in full progress. During this transition, technologies such as plug-in hybrid (PHEV), full hybrid (FHEV) and mild hybrid (48V - MHEV) are common "hybrid" solutions. Li-Ion based and other energy storage technologies are constantly being improved as an energy storage solution for hybrid electric vehicles and other systems. Other well-known technologies such as NiMH based energy storage systems (ESS) are still being used. For ESS an effective and precise State of Charge estimation (SOC) is mandatory. However, hysteresis effects underlying technologies, caused by chemical and physical processes, make it difficult to determine the SOC accurately.

Current state-of-the-art models discussed in [1] are based on physical/electrical [2]–[6] or mathematical/analytical [1], [7]–[11] approaches. The higher the accuracy needed (< 2 %), the more complex the model has to be thus leading to more computational and experimental efforts to validate and implement the model into diagnostic devices. As an example, in order to take relaxation phases along with hysteresis effects into account, a number of at least four RC-branches in series within equivalent circuit models is required to achieve an error lower than 2 % [3].

With a new controller-based approach, inspired by watching drones recognizing and following a path, the complex process for modeling and implementation of SOC estimation was reduced to such an extent that a broader range of experts could have access to this important area.

# 2   Fundamentals and state of the art

## 2.1   Hysteresis and Modelling

What is meant by the term hysteresis is explained in detail in [12]. Systems with hysteresis are non-linear, have a discontinuous transfer characteristic and thus represent a challenge for modelling. Hysteresis can be both rate-dependent, e.g. systems with lag, and rate-independent, e.g. ferromagnetism.

Since an overview of the state of the art of hysteresis modelling is already given in[1] only a short overview of the different approaches to the simulation of hysteresis curves and their error rates shall be given here.

*Mathematical models* try to reproduce the hysteresis curves of systems or objects. It is difficult to develop general models for all kinds of curve shapes. There are approaches that try to combine physical system properties with parameters of mathematical equations [8].

*Electrical/physical models* attempt to model the physics and behaviour of systems affected by hysteresis using equivalent circuit diagrams. The mathematical relationship is established by the components used, such as capacitors, whose charge and discharge curves are described by a previously defined function. Thus a system is more or less graphically modelled with function blocks instead of equations. Therefore the result of both approaches is often very similar depending on the effort involved. Depending on the application, however, it can be advantageous to use one or the other approach

A third approach is represented by control theory. A controller (Figure 1) represents a numerical, self-regulating (with feedback) process with a mathematical, deterministic behaviour. Applications that are difficult to describe mathematically can be handled with a numerical approach. The system is allowed to operate within certain limits, and the controller is set to operate automatically within these limits. The control dynamics always result in a hysteresis, which has a local or non-local memory depending on the controller design [12]. A controller can simulate both rate-dependent and rate-independent behaviour. Two-step and multistep controllers belong to the non-linear controllers and can be used to model hysteresis curves, for example.
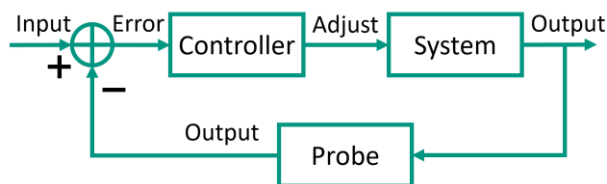


Figure 1: Block diagram of a simple standard control loop with feedback

### 2.1.1   Hysteresis Curve and Eye Effect

A hysteresis is not only characterized by the boundary curves (main loop), but also by intermediate sub-hysteresis loops (minor loops) (see Figure 2). During continuous charging or discharging, the open-circuit voltage (OCV) follows the major curve. However, in incomplete charge/discharge cycles with subsequent relaxation or discharge/charge phases, the OCV follows the minor loops between the boundaries of the major loop. Because of reversible system processes, a hysteresis loop is generally symmetrical. But due to additional processes, e.g. losses at different SOC levels, the major hysteresis curve in such a region can be distorted as well as the minor loops. Therefore it is not easy to model such a distorted hysteresis curve using equations only. In complex cases,

the major and minor hysteresis loops of a system must be measured and stored in a look-up table for later simulations. This can require a lot of effort and high costs.
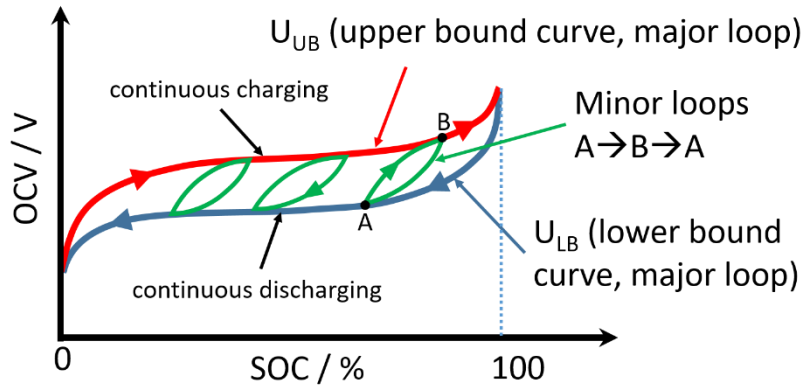


Figure 2: Energy storage with hysteresis, like NiMH based batteries

### 2.1.2    Model 1 Preisach

In this section, just a short summary of the Preisach model for hysteresis is given, for a more detailed explanation of the model see [1], an example of discrete implementation in [13], or for a complete discussion on Preisach model see [7]. The Preisach model is a widely accepted general mathematical tool to describe various hysteresis phenomena.

The Preisach model divides the area between the upper and lower boundary curve (Figure 2) into areas with hard-switching "two-point controllers" called Hysterons [7]. The weighting of these distributed Hysterons is represented by a function and must be determined separately for each hysteresis affected system.

In software applications, a discrete version is used in which the continuous integral in the Preisach triangle T is replaced by a sum of N areas, the distribution of which is represented by the weighting function $\mu(\alpha, \beta)$ [7].

The accuracy of the discrete Preisach model depends on two factors. First, the resolution when measuring the Preisach distribution function for the model and second, the number of Hysterons used in the model to calculate the output function. Thus, the accuracy of the Preisach model depends directly on the available system resources [13].

### 2.1.3    Jiles-Atherton Model

The Jiles-Atherton model [8] is very popular for many applications, because it combines physical system properties with parameters of a generalized mathematical equation. For the different aspects of a hysteresis curve, (linear section, saturation phase, minor loop, etc.) additional equations are formulated in this model and linked under certain conditions. The model is able to simulate major and minor hysteresis loops, and static and dynamic hysteresis.

### 2.1.4    Takács Model

The model proposed by Takács [9] was inspired by the Langevin function but takes a different approach. In this model, a function on a tangent hyperbolic basis is used to describe the hysteresis curve as a generalized function. By means of various parameters, it is possible to modify the basic function and thus to adapt the appearance of the hysteresis curve to the respective application. It is also possible to model minor loops by extending the basic equation. As with most generalized mathematical models, the underlying equations are sometimes very extensive

and complicated. A software application would therefore be very costly with only a small gain in accuracy compared with the discrete Preisach model, for example.

### 2.1.5    Electrical equivalent model based on Thevenin battery model

The equivalent circuit diagram according to Thevenin [14] is often used to model an energy storage device with hysteresis (Figure 3). With $R_i$ the internal resistance and $U_{OC}$ the open circuit voltage of the battery, $C_0$ the battery capacity and $R_0$ the polarization resistance (transition resistance between the electrodes and the electrolyte).

Depending on the complexity, one, two or even more R‖C elements are used to model the behaviour of the energy storage system. The more R‖C elements are used, the more effort is required to determine the parameters for the individual resistances and capacitances. In the following two approaches are briefly described how the parameters of such complex electrical equivalent circuits can be identified.
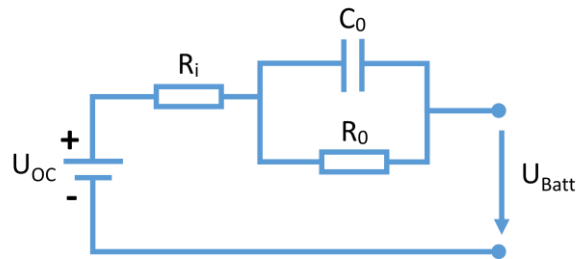


Figure 3: Thevenin battery model

**Thele and Sauer** [2]: The model presented by Thele and Sauer investigates and measures the impedance spectrum of an energy storage device using Electrochemical Impedance Spectroscopy (EIS) and thus identifying the parameters for the electrical equivalent circuit diagram. Various losses during charging and discharging of the energy storage device are modelled with separate equations.

For the representation of hysteresis, for example in NiMH based batteries, an additional numerical hysteresis model is integrated additionally to the Thevenin model. A 5th order polynomial with SOC as input variable models the upper and lower bound curves shown in Figure 2. Minor loops between the upper and lower bound curves are generated and modelled using interpolation points. This process is very complex in a software implementation and offers low error rates only with ideal static hysteresis curves.

**Pelissier** [3]: The model presented by S. Pelissier et. al. is concerned with the observation and investigation of the relaxation curves for various energy storages to identify the respective equivalent circuit parameters. The very long relaxation phases are approximated with exponential functions to identify the parameters for three and more R‖C elements in the system. The error rate decreases with the number of R‖C elements used. However, the parameterization and implementation effort for the model increases.

## 2.2    Gassing

A typical NiMH cell consists of a positive NiOOH / Ni(OH)2 electrode and a slightly larger negative metal hydride electrode. The overcharge (OCR) and overdischarge reservoirs (ODR) form areas that provide space for recombination of the gases produced during overcharge and deep discharge (Figure 4). Thus the battery can withstand many cycles and is not immediately destroyed if it is overcharged or deeply discharged.

The modelling of energy losses due to the gassing reactions has already been explained in detail in [2]. The model presented in this paper uses the equation and parameters from [2] to estimate the gassing losses. Measurements on the test cells have shown that even at low currents and a SOC level of like 70% and above, increased oxygen formation can occur. Therefore, it is not so trivial to simulate the gassing losses with a high accuracy. The equation

used in [2] has already given some good results, but needs further investigation and adaptation for the model when using long profiles (6 - 40 h).
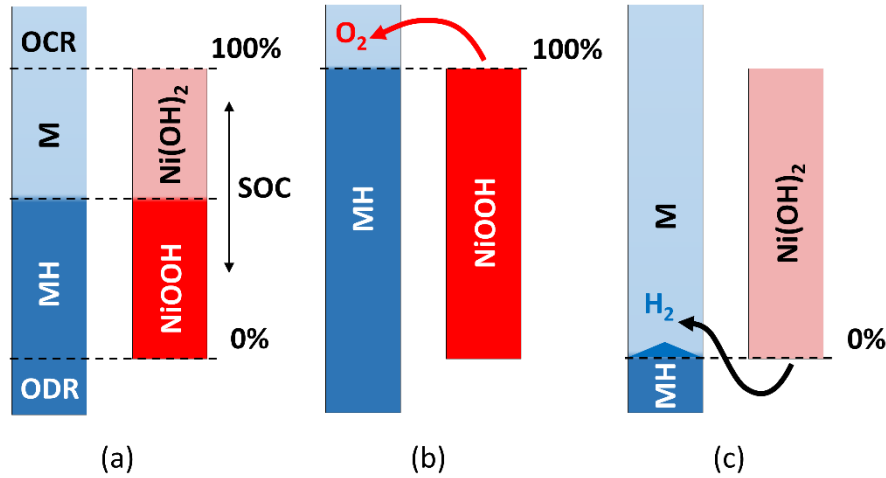


Figure 4: Typical NiMH Cell Design. a) regular operation, b) overcharge state, c) overdischarge state (derived from [15])

# 3  Method

## 3.1  Characteristic Cell

The test cells used are prototypes of a commercial NiMH based hybrid energy storage. Working title within this paper will be HybridCap.

Table 1: Data of the HybridCaps

| Name | Value |
|---|---|
| Rated Voltage Range | 0.8 - 1.45 V |
| Rated Capacity | 4.5 Ah |
| Rated Ri (DC) | 2 m$\Omega$ |

## 3.2  PID-Controller approach

RC elements are used in most physical/electrical models as it is possible to divide all modelled processes into damped charging and discharging processes. The mathematical models addressed in the fundamentals chapter partly follow a similar approach.

The damped charging and discharging can be represented mathematically through an exponential function. If one considers the step response of a simple P controller, strong similarities between the exponential function and the step response can be observed depending on the setting of the controller dynamics. Basically the hysteresis effect occurs due to inertia, lagging or asymmetry of reversible processes, like in the case of NiMH based ESS the chemical and physical processes during charge/discharge.

As energy storage technology based on NiMH is strongly affected by hysteresis effect, this type of energy storage in form of a cylindrical high power hybrid capacitor is used for the study. For the model, the major hysteresis

curve (upper and lower bound) is measured by a constant charge/discharge from 0 to 100 % SOC and is provided in a look-up table. This is actually a crucial part of this model. The controller parameters are set due to repeating charge/discharge loops within the major hysteresis curve.

Figure 5 describes the operating principle of the controller-based hysteresis model. Considering losses due to the internal resistance $R_i$ and gassing for NiMH as it is decribed in [2] for the input current $I_{input}$, an Ampere-hour counting method with respect to the nominal capacity is used to calculate the SOC, which is needed to determine the voltage set point $U_{input}$ on the major hysteresis curve for the controller (Figure 6).

The following adjustment made by the controller is represented by $U_{adj}$ and is added to the actual voltage of the ESS resulting in the output voltage $U_{out}$. A feedback probe connects the output with the input and calculates the error between them. The error is then provided to the controller input.
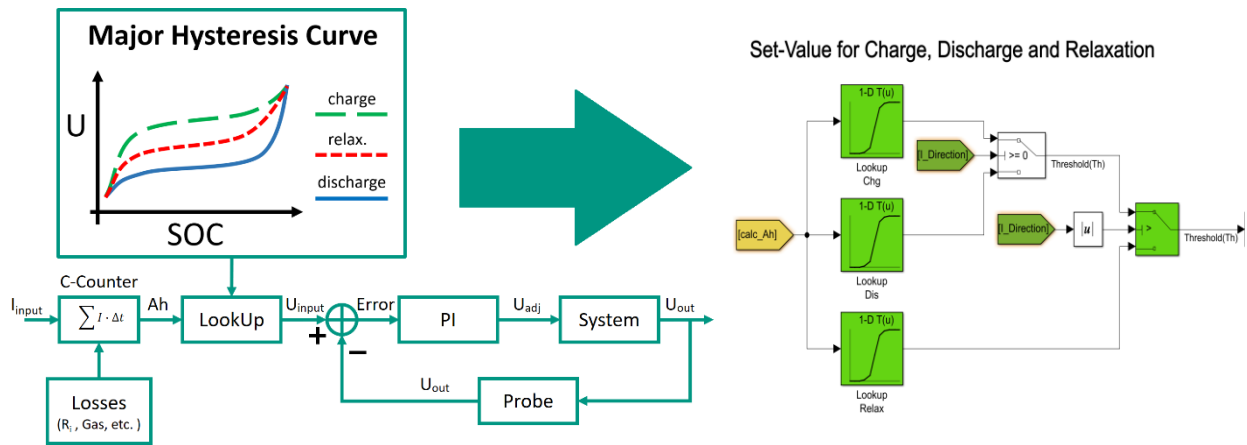


Figure 5: Diagram of the Hysteresis Model with Controller integration, with the Simulink implementation on the right side
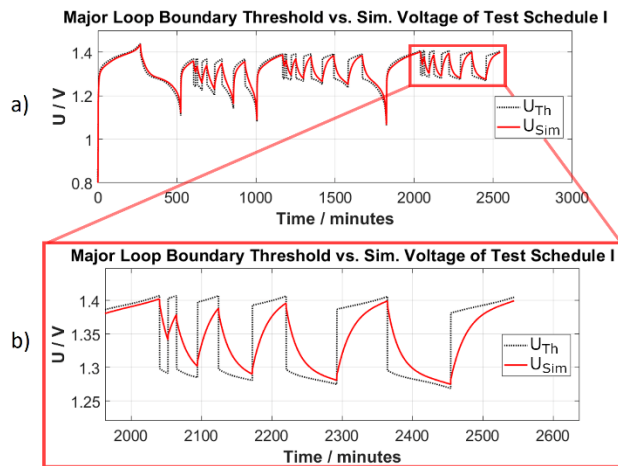


Figure 6: a) set point voltage ($U_{Th}$) for controller input and followed simulated voltage ($U_{Sim}$), b) zoomed part of a)

One goal of this proposed model is to estimate the battery OCV, when the battery voltage follows a minor loop, and then use the OCV - SOC relationship to calculate the estimated SOC from the OCV. The SOC estimation

related to the OCV and the ampere hour accumulation could be combined in a future work using a Kalman filter for a better estimation of the SOC.

The current model does not take into account cell aging and temperature fluctuations. The gassing function from [2] also requires further investigations and adjustments for the model presented here.

# 4 Analysis / Validation

This section describes the experimental setup used to obtain data for the validation of the proposed model in this work. A brief summary of the objectives of each schedule is presented in Table 2. The tests were done in the battery lab with testing devices and cell setup as shown in Figure 7. Figure 8 shows the test procedure carried out for Schedule I and II. Schedule III was derived from the dynamic stress test (DST) profile intended for the performance evaluation of an energy storage for automotive applications.

The load profile used in Schedule I served as a training profile for the presented model to find the parameters for the controller (look-up tables for the set point values, gain factors $K_P$ and $K_I$ for the proportional and integral part) and the losses during charging and discharging. Schedule II and Schedule III were used to validate the model.
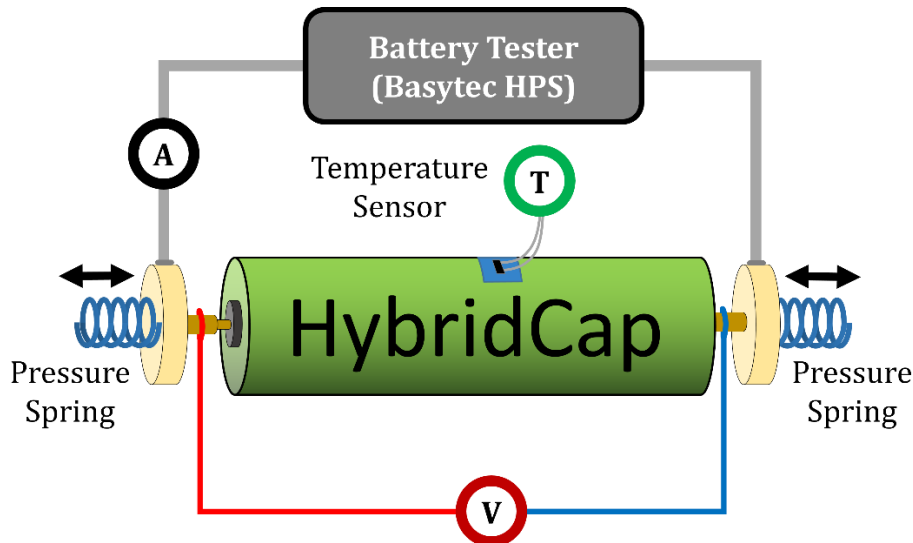
Figure 7: Experimental setup

In all schedules the cells were completely discharged before the test procedures were started. The test profile shown in Figure 9 and Figure 11 was performed at a Start SOC of 30 %, 60 % and 80 % respectively (Start schedule: 0 % → 100 % → 0 % → Start SOC → Test procedure). The procedure for the DST profile is described in [16] in detail.

All measurements for Schedules I - III were performed at an ambient temperature of 25°C and a charge-discharge current of 1 A (0.2 C). The test profiles used are shown in Figure 9, Figure 11 and Figure 12.

Start SoC → #1 ±0.2Ah → #2 ±0.5Ah → #3 ±0.8Ah → #4 ±1.2Ah → #5 ±1.5Ah → Start SoC
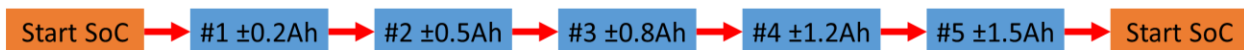
Figure 8: Procedure for test Schedule I and II

Table 2: Brief summary description of the schedules

| Schedule | Info | Test Profile |
|---|---|---|
| I | Training, identification of controller parameter and system losses, minor loop tests | Procedure shown in Figure 8, profile used shown in Figure 9 |
| II | Model validation, minor loop tests | Procedure shown in Figure 8, profile used shown in Figure 11 |
| III | Model validation on a DST Profile with parameters from Schedule I | Profile used shown in Figure 12, detailed profile explanation in [16] |

As an example, the test profile for Schedule I, performed with the Basytec HPS device, is shown below in Figure 10. To illustrate the relationship between the profile sections in Schedule I (major loop, 30 %, 60 % and 80 % SOC), the colours used in Figure 10 under the column "Info" are the same as those used in Figure 13 and Figure 14.
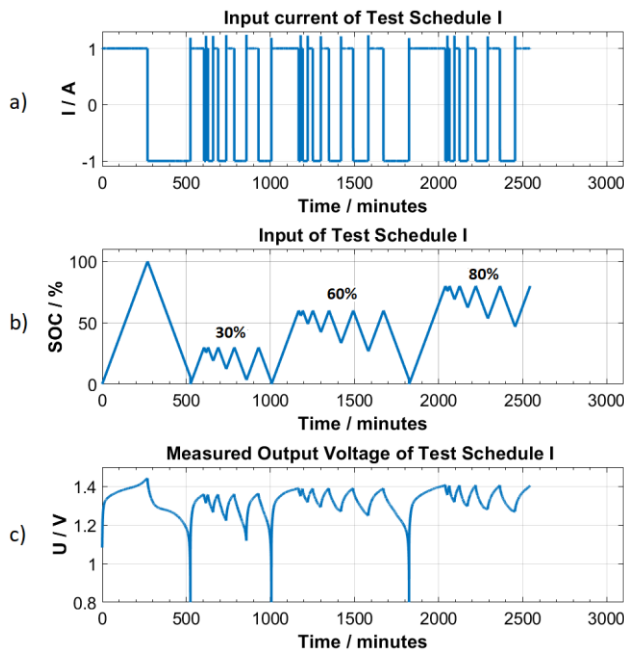


Figure 9: Input-output of test Schedule I with a) current, b) SOC and c) voltage

| Profile state | Profile parameter | Condition | Info |
|---|---|---|---|
| Start | | | |
| | | | complete discharge from unknown SOC state |
| discharge | I=1A | U<0.8V | |
| charge | I=1A, U=1.45V | I<0.05A, Ah>4.5Ah | measurement of major loop |
| discharge | I=1A | U<0.8V | |
| charge | I=1A | Ah>1.35Ah | |
| discharge | I=1A | Ah<-0.2Ah | |
| Charge | I=1A | Ah>0.2Ah | |
| Discharge | I=1A | Ah<-0.5Ah | |
| Charge | I=1A | Ah>0.5Ah | |
| Discharge | I=1A | Ah<-0.8Ah | |
| Charge | I=1A | Ah>0.8Ah | |
| Discharge | I=1A | Ah<-1.2Ah | |
| Charge | I=1A | Ah>1.2Ah | End 30% SOC Test |
| discharge | I=1A | U<0.8V | discharge to 0% SOC |
| charge | I=1A | Ah>2.7Ah | |
| discharge | I=1A | Ah<-0.2Ah | |
| Charge | I=1A | Ah>0.2Ah | |
| Discharge | I=1A | Ah<-0.5Ah | |
| Charge | I=1A | Ah>0.5Ah | |
| Discharge | I=1A | Ah<-0.8Ah | |
| Charge | I=1A | Ah>0.8Ah | |
| Discharge | I=1A | Ah<-1.2Ah | |
| Charge | I=1A | Ah>1.2Ah | |
| Discharge | I=1A | Ah<-1.5Ah | |
| Charge | I=1A | Ah>1.5Ah | End 60% SOC Test |
| discharge | I=1A | U<0.8V | discharge to 0% SOC |
| charge | I=1A | Ah>3.6Ah | |
| discharge | I=1A | Ah<-0.2Ah | |
| Charge | I=1A | Ah>0.2Ah | |
| Discharge | I=1A | Ah<-0.5Ah | |
| Charge | I=1A | Ah>0.5Ah | |
| Discharge | I=1A | Ah<-0.8Ah | |
| Charge | I=1A | Ah>0.8Ah | |
| Discharge | I=1A | Ah<-1.2Ah | |
| Charge | I=1A | Ah>1.2Ah | |
| Discharge | I=1A | Ah<-1.5Ah | |
| Charge | I=1A | Ah>1.5Ah | End 80% SOC Test |
| Stop | | | |

Figure 10: Complete teste profile of Schedule I
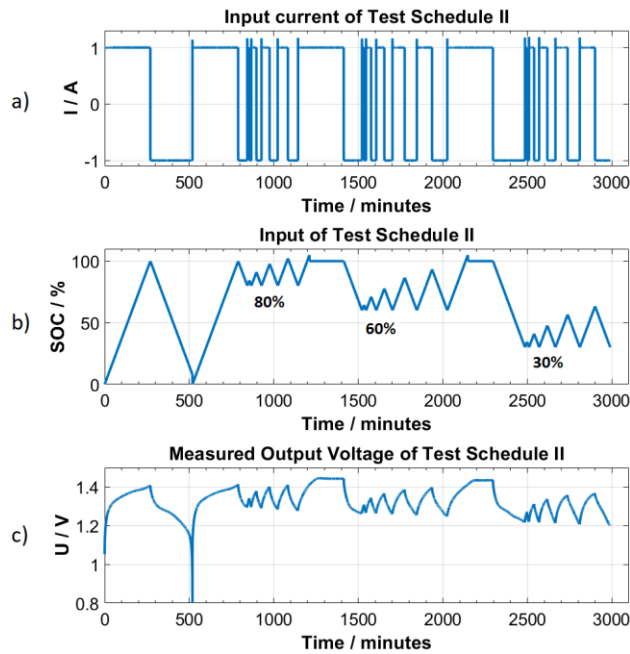
Figure 11: Input-output of test Schedule II with a) current, b) SOC and c) voltage
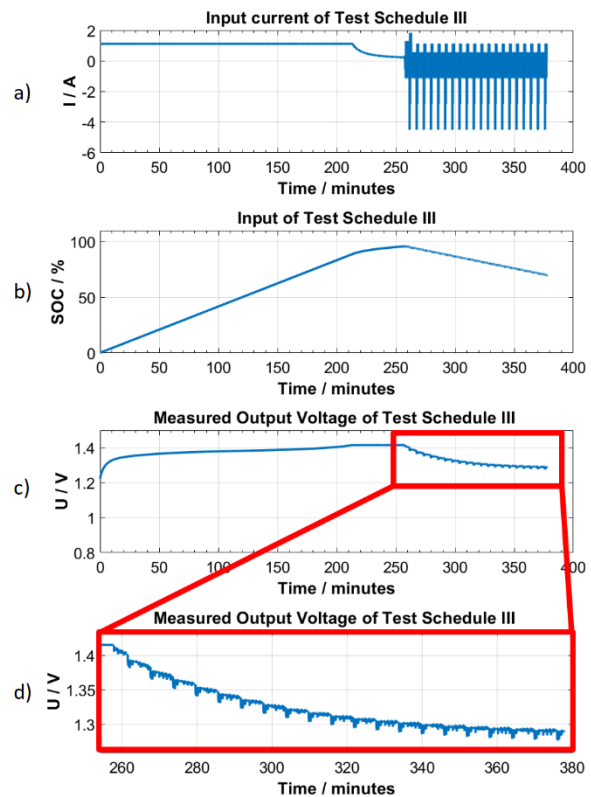


Figure 12: Input-output of test Schedule III with a) current, b) SOC, c) voltage and d) zoomed voltage of DST part

## 5 Results

In this section the results and root mean square (RMS) error of the test Schedules I - III are presented.

The Schedules I - III were not performed with new cells, but with differently aged cells. Therefore a modified major loop was used for all simulations, which was calculated from the mean values of all measured major loops of the individual cells. This increases the RMSE of the voltage by approx. 1 %, but serves to simplify the model and allows the simulation of different test scenarios even with partially incomplete measurement data. For example the DST profile in Schedule III, for which no major loop data is available. $U_{Ref}$ represents the measured voltage and $U_{Sim}$ the simulated voltage.

The SOC in Schedule I and II is very well replicated by the ampere hour counter compared to Schedule III. The RMSE here is well below 1% (Figure 13 and Figure 14). The reason for this may be that the charge and discharge current in Schedule I and II is kept low at 0.2 C and the occurring losses are to some extent linear. In the DST profile in Schedule III the current varies between +0.2 C and -1 C. The RMSE here is significantly higher with 2.1 % (Figure 16). The model therefore needs further adaptation at this point.
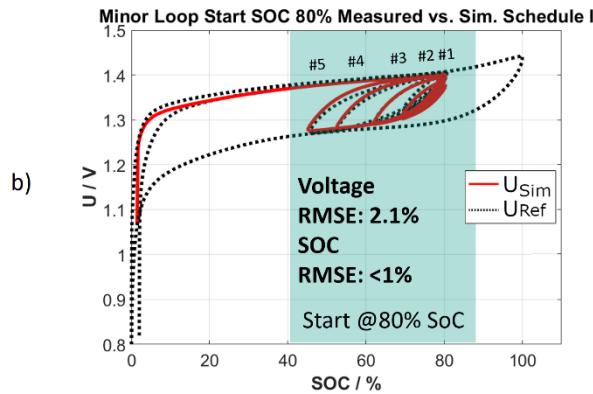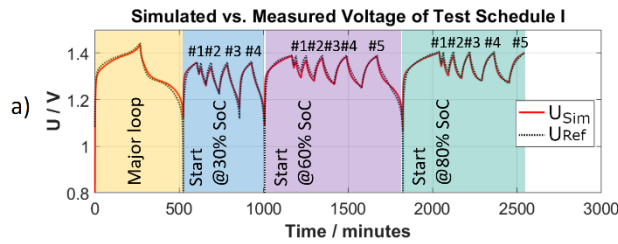
Figure 13: Minor Loops with 30, 60, 80 % Start SOC with a) voltage and b) minor loops
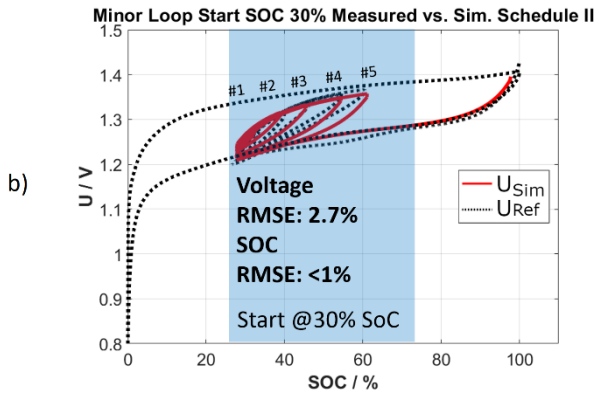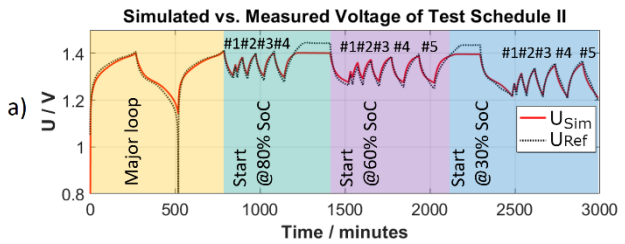
Figure 14: Minor Loops with 80, 60, 30 % Start SOC with a) voltage and b) minor loops
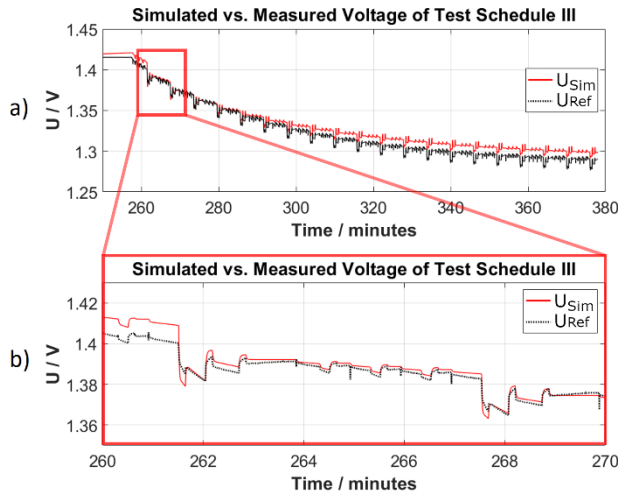


Figure 15: a) Simulation of Test Schedule III Voltage, b) zoomed part of a)
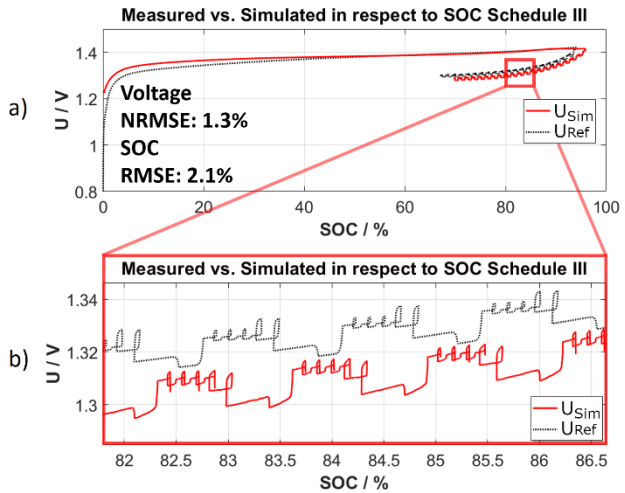
Figure 16: a) Simulation of Test Schedule III SOC b) zoomed part of a)

**Comparison of the RMSE of the other approaches mentioned here in this paper:**

**Discrete Preisach** [13]: low Resolution 5 - 10 % RMSE, low computational effort, high Resolution 1 - 2 % RMSE, high computational effort.

**Thele, Sauer model**: 1 - 2 % RMSE without gassing function.

**Pelissier**: dependent on the number of R‖C elements in the model between 8 % and <1 % for two R‖C elements or 5 and more R‖C elements respectively.

**Takács**: SOC RMSE between 4 - 6 % with some significant computational effort.

**Jiles-Atherton**: There are computational problems with the model in software applications. Therefore the use of a neural network was proposed to identify the parameters of the JA model, where the measured hysteresis curve serves as input for the network. Then the error could be within 5 % RMSE [17].

# 6    Conclusion

For each test-call a complete charge/discharge cycle should be performed and the measured OCV of the particular cell should be stored in separate loop-up tables, to be used only with that cell. Therefore the look-up data for the major curves used in the model and the real OCV of the particular cells are as similar as possible. This should minimize the error of the model. In an application, the SOC algorithm is calibrated using his own system battery and is re-calibrated each time the battery is swapped out.
The introduced controller-based approach achieves a normalized root mean square error (NRMSE) of around 2-3 % combined error for voltage and SOC, which is comparable to high complex RC models of the literature.
With its flexibility in parametrization and field of application, the model can be used in nearly all cases where hysteresis effects occur, e.g. for other storage technologies like LiFePO4 (LFP) or within magnetism.

The implementation of a neural network into the model could be considered to help with the simulation of various noise inputs to the control loop, like aging or temperature variation. This could also improve the actual SOC prediction in electric vehicles.

# Acknowledgments

# References

[1]   F. Baronti, N. Femia, R. Saletti, C. Visone, und W. Zamboni, „Preisach modelling of lithium-iron-phosphate battery hysteresis", *J. Energy Storage*, Bd. 4, S. 51–61, 2015, doi: 10.1016/j.est.2015.09.004.

[2]   M. Thele, O. Bohlen, D. U. Sauer, und E. Karden, „Development of a voltage-behavior model for NiMH batteries using an impedance-based modeling concept", *J. Power Sources*, Bd. 175, Nr. 1, S. 635–643, 2008, doi: 10.1016/j.jpowsour.2007.08.039.

[3]   A. Li, S. Pelissier, P. Venet, und P. Gyan, „Fast Characterization Method for Modeling Battery Relaxation Voltage", *Batteries*, Bd. 2, Nr. 2, S. 7, 2016, doi: 10.3390/batteries2020007.

[4]   M. Verbrugge und E. Tate, „Adaptive state of charge algorithm for nickel metal hydride batteries including hysteresis phenomena", *J. Power Sources*, Bd. 126, Nr. 1–2, S. 236–249, 2004, doi: 10.1016/j.jpowsour.2003.08.042.

[5]   R. Lu, T. Wang, F. Feng, und C. Zhu, „SOC Estimation Based on the Model of Ni-MH Battery Dynamic Hysteresis Characteristic", *World Electr. Veh. J.*, Bd. 4, Nr. 2, S. 259–265, Juni 2010, doi: 10.3390/wevj4020259.

[6]   Y. Ota und Y. Hashimoto, „Modeling of voltage hysteresis and relaxation of HEV NiMH battery", *Electr. Eng. Jpn.*, Bd. 175, Nr. 1, S. 1–7, 2011, doi: 10.1002/eej.21102.

[7]   I. D. Mayergoyz, *Mathematical Models of Hysteresis and their Applications*, 2nd ed. Burlington: Elsevier, 2003.

[8]   D. C. Jiles und D. L. Atherton, „Theory of ferromagnetic hysteresis (invited)", *J. Appl. Phys.*, Bd. 55, Nr. 6, S. 2115–2120, 1984, doi: 10.1063/1.333582.

[9]   J. Takács, „A phenomenological mathematical model of hysteresis", *COMPEL - Int. J. Comput. Math. Electr. Electron. Eng.*, Bd. 20, Nr. 4, S. 1002–1015, 2001, doi: 10.1108/EUM0000000005771.

[10] L. Zhu, Z. Sun, H. Dai, und X. Wei, „A novel modeling methodology of open circuit voltage hysteresis for LiFePO 4 batteries based on an adaptive discrete Preisach model", *Appl. Energy*, Bd. 155, S. 91–109, 2015, doi: 10.1016/j.apenergy.2015.05.103.

[11] M. L. Grimmer, „Analysis of Hysteretic Systems: Preisach Formalism and Bouc-Wen Modeling", Thesis, 2017.

[12] G. Bertotti, *Hysteresis in magnetism: For physicists, materials scientists and engineers*, Digitaler Nachdr. San Diego, Calif.: Acad. Press, 2008.

[13] P. Chayratsami und G. L. Plett, „Hysteresis Modeling of Lithium–Silicon Half Cells Using Krasnosel'skii-Pokrovskii Model", in *2019 IEEE Conference on Control Technology and Applications (CCTA)*, 2019, S. 470–475, doi: 10.1109/CCTA.2019.8920524.

[14] H. He, R. Xiong, und J. Fan, „Evaluation of Lithium-Ion Battery Equivalent Circuit Models for State of Charge Estimation by an Experimental Approach", *Energies*, Bd. 4, Nr. 4, S. 582–598, 2011, doi: 10.3390/en4040582.

[15] K. Young, *Nickel metal hydride batteries*. Basel: MDPI AG - Multidisciplinary Digital Publishing Institute, 2016.

[16] G. Mulder, „Test methods for improved battery cell understanding: Draft White Paper", 2018, [Online]. Verfügbar unter: https://www.batterystandards.info/literature.

[17] M. Trapanese, V. Franzitta, und A. Viola, „The Jiles Atherton model for description of hysteresis in lithium battery", in *Twenty-Eighth Annual IEEE Applied Power Electronics Conference and Exposition (APEC), 2013*, Piscataway, NJ, 2013, S. 2773–2775, doi: 10.1109/APEC.2013.6520689.

## Authors

Sergej Koch was born in Kotowo, UDSSR. He received the Dipl.-Ing degree in electrical engineering from the University of applied science in Pforzheim, Germany, in 2009. Starting in 2010, he had a Start-Up company for developing signal measurement and communication devices for underwater use. Since 2018 he got an opportunity to start with the research and development of software models for NiMH-based storage systems and the simulation of new battery systems solutions, like passive hybrid ESS with battery and super capacitor components, at the Karlsruhe Institute of Technology (KIT), Karlsruhe, Germany.
His further mission at KIT is the validation and development of systems to optimize and increase the yield of new and existing photovoltaic systems.

Thorsten Grün was born in Weert, Netherlands. He received the Dipl.-Ing degree in power systems technology from Clausthal University of Technology, Clausthal, Germany, in 2014. Since 2014 he is working at the Karlsruhe Institute of Technology, Karlsruhe, Germany.
His research interests include the experimental and model-based investigation of lithium-ion batteries and super capacitors on cell and system level and the design of hybrid storage systems.

Martin Doppelbauer was born in Altenhundem, Germany. He received the Dipl.-Ing. and Dr.-Ing. degrees in electrical engineering from the University of Dortmund, Dortmund, Germany, in 1990 and 1995, respectively.
He has worked with the companies Danfoss Bauer, Esslingen, and SEW Eurodrive, Bruchsal, Germany, as a Senior Manager for electric motor development. He has been holding the Professorship for hybrid electric vehicles at the Karlsruhe Institute of Technology, Karlsruhe, Germany, since 2011.